P13 **MITIGATING EXCESSIVE DRYING CAUSED BY OBSERVATION NUDGING**

Brian P. Reen*, Robert E. Dumais, Jr., and Jeffrey E. Passner
Battlefield Environment Division, U.S. Army Research Laboratory

1. INTRODUCTION

Observations are often used to enhance the initial conditions in a mesoscale model to improve the subsequent model forecast. However, in order to utilize observations made at discrete points to improve a three-dimensional model, one must make certain assumptions about error correlation. Assimilation of moisture information can pose particular difficulties due to the high spatial variability of mixing ratio (and specific humidity) relative to the absolute value of mixing ratio (and specific humidity) (e.g., Dee and da Silva 2003). We illustrate how the introduction of observations into the initial conditions can cause the initial conditions to be excessively dry, and demonstrate solutions to the over drying.

Various techniques are available to utilize observations in the initial conditions including those that introduce changes at discrete times (intermittent) and those that gradually adjust the model solution over many time steps (continuous). Here we gradually nudge the model towards observations (observation nudging; Deng et al. 2009; Stauffer and Seaman 1994) during a pre-forecast in order to improve the conditions used to start the free forecast. This technique is conceptually simple, relatively inexpensive computationally, and allows the dynamic balance and intervariable consistency of the model to be maintained (Ardao-Berdejo and Stauffer 1996; Seaman 2000). We also use the flow dependent multi-scan Cressman analysis method in Obsgrid to incorporate observations into the model conditions at the beginning of the pre-forecast.

2. MODEL DESCRIPTION AND CONFIGURATION

The Advanced Research version of the Weather Research and Forecasting model (WRF-ARW) v3.4.1 (Skamarock et al. 2008) was configured with 9-km horizontal grid spacing centered over southern California and 56 vertical layers. The model was integrated from 12 UTC to 12 UTC for the five case days described in Section 3. The observation nudging capability of WRF (Deng et al. 2009) is used to incorporate observations into the model via a 6-hour pre-forecast (12 to 18 UTC).

*Corresponding author address: Brian P. Reen, Army Research Laboratory, 2800 Powder Mill Road, Adelphi, MD 20783; e-mail: brian.p.reen.civ@mail.mil

Global Forecast System (GFS) 0.5-degree horizontal resolution output is used to create initial conditions and boundary conditions. A higher-resolution product from the National Centers for Environmental Prediction, Marine Modeling and Analysis Branch, called the Real Time Global Sea Surface Temperature (Genmill et al. 2007) has $1/12^{th}$ degree horizontal grid spacing and was used to specify sea surface temperatures. Where available, GFS snow fields were replaced with 1-km snow fields from the National Weather Service's National Operational Hydrologic Remote Sensing Center (NOHRSC) SNow Data Assimilation System (SNODAS; National Operational Hydrologic Remote Sensing Center, 2004).

The Mellor-Yamada-Janjić scheme (MYJ; Janjić 2002) is used to parameterize the atmospheric boundary layer. As in Lee et al. (2012), the background turbulent kinetic energy (TKE) is decreased to better simulate conditions with low TKE and the ABL depth diagnosis is altered. In preliminary experiments for this study, the standard MYJ scheme resulted in noisy TKE fields and thus noisy ABL depth fields over the water. These were resolved using the altered version of MYJ. The other parameterizations utilized included the WRF single-moment 5-class microphysics parameterization, the Kain-Fritsch cumulus parameterization, the Rapid Radiative Transfer Model for longwave radiation and the Dudhia scheme for shortwave radiation. The Noah land surface model is used to represent land surface processes.

3. CASE DESCRIPTION

Five 24-hour periods from early 2012 over the southwestern United States were examined which started at 12 UTC on: 7 February, 9 February, 16 February, 1 March, and 5 March. The case days were chosen to include both days with active weather and days with more benign weather. Widespread precipitation occurred on 7 February, while more limited precipitation occurred on 16 February and 1 March. More quiescent weather occurred for the 9 February and 5 March cases.

4. METHODOLOGY

4.1 Dewpoint Climatology

In order to determine whether model water vapor fields were unrealistically dry, a dewpoint climatology was constructed using rawinsonde data. All rawinsonde data for January, February, and March for 1990-2012 at four locations within the model domain are included: Oakland, California, San Diego, California, Tucson,

Arizona, and Desert Rock, Nevada. Desert Rock did not take upper-air observations in 2011 or 2012. For each 50-hPa bin, the lowest 0.1- percentile dewpoint among the four locations was chosen to create a vertical profile of dewpoints.

4.2 Observation Data Sources

Observations from the Meteorological Assimilation Data Ingest System (MADIS; madis.noaa.gov) database as well as Tropospheric Aircraft Meteorological Data Reports (TAMDAR; e.g., Gao et al. 2012) observations were used for data assimilation. The MADIS data include standard surface observations, as well as mesonet data, maritime observations, profiler data, aircraft data, and rawinsondes. It was found that insufficient quality control could result in observation nudging including "bad" observations and lead to areas with unrealistically dry conditions. Therefore, Obsgrid was used as the primary source of quality control. In addition to the Obsgrid quality control procedures, the Real Time Mesoscale Analysis (RTMA; De Pondeca et al. 2011) use/reject lists were used to filter the mesonet data.

4.3 Nudging Technique

Observation nudging adds a non-physical term to the tendency equations, and is implemented in WRF as:

$$\frac{\partial q\mu}{\partial t}(x,y,z,t) = F_q(x,y,z,t) + \mu G_q \frac{\sum_{i=1}^{N} W_q^2(i,x,y,z,t)\left[q_o(i) - q_m(x_i,y_i,z_i,t)\right]}{\sum_{i=1}^{N} W_q(i,x,y,z,t)}$$

where q is the quantity being nudged (e.g., water vapor mixing ratio), μ is the dry hydrostatic pressure, F_q represents the physical tendency terms of q, G_q is the nudging strength for q, N is the total number of observations, i is the index to the current observation, W_q is the spatiotemporal weighting function, q_o is the observed value of q, and $q_m(x_i,y_i,z_i,t)$ is the model value of q interpolated to the observation location. The quantity q_o-q_m is the innovation. In the standard WRF observation nudging code surface observations reported as part of a sounding are treated as another layer in the sounding; we instead assimilate these surface observations as surface observations and do not include them as the lowest level in the sounding. This allows these surface observations to be applied at the surface and to be spread along the surface rather than being assimilated in pressure space.

We investigate preventing observation nudging from nudging towards a negative value of water vapor mixing ratio. When applying a negative moisture innovation, we implement this by ensuring that the magnitude of the innovation does not exceed the model water vapor mixing ratio at the model point at which the innovation is applied. The methodology can also be expressed as follows. When applying an observation $q_0(i)$ to (x,y,z,t) if:

$$\left\{\left[q_o(i) - q_m(x_i,y_i,z_i,t)\right] < 0\right\} \wedge \left\{q_m(x,y,z,t) < q_m(x_i,y_i,z_i,t)\right\}$$

then the nudging equation becomes:

$$\frac{\partial q\mu}{\partial t}(x,y,z,t) = F_q(x,y,z,t) + \mu G_q \frac{\sum_{i=1}^{N} W_q^2(i,x,y,z,t) I_a}{\sum_{i=1}^{N} W_q(i,x,y,z,t)}$$

where:

$$I_a = \max\left\{\left[q_o(i) - q_m(x_i,y_i,z_i,t)\right], -q_m(x,y,z,t)\right\}$$

4.4 Initial Condition Enhancement

For some experiments we use initial conditions generated by incorporating observations onto the GFS fields through a modified Cressman analysis with Obsgrid. The Cressman analysis is applied through a series of four scans with successively smaller radii of influence. The area a given wind or moisture observation influences is a "banana" shape following the wind flow (this reduces to an ellipse in non-curved flow and a circle in weak-wind conditions).

We investigate modifying the Cressman analysis in Obsgrid for relative humidity to limit its introduction of very dry conditions. If an observation at point A ($RH_{ob,A}$) is dryer than the first guess field at point A ($RH_{fg,A}$), and the first guess field at point B ($RH_{fg,B}$) is dryer than the first-guess field at point A, then the changes to the first-guess field at point B are scaled. Namely, the ratio of the first-guess value at point B to that at point A is used to scale the drying instituted at point A. This means that for a case with a single observation at point A, when applying this observation to the analysis at point B, if:

$$\left(RH_{fg,A} > RH_{ob,A}\right) \wedge \left(RH_{fg,B} < RH_{fg,A}\right)$$

then:

$$RH_{an,B} = RH_{fg,B} + F * \left(\frac{RH_{fg,B}}{RH_{fg,A}}\right)\left(RH_{ob,A} - RH_{fg,A}\right)$$

Else:

$$RH_{an,B} = RH_{fg,B} + F * \left(RH_{ob,A} - RH_{fg,A}\right)$$

where F is the distance weighting. For the first scan (largest radius of influence), the first-guess field is GFS, but for subsequent scans the first-guess field is the end result of the previous scan.

5. EXPERIMENTAL DESIGN

A control experiment using GFS data as initial conditions and having no data assimilation (Exp. Control) is compared to a set of experiments that varies the initial conditions and the data assimilation configuration.. These experiments were completed on all five case days and are listed in Table 1.

The initial conditions were created using three options. Exp. Control used the GFS fields for the initial conditions. The standard Cressman analysis scheme in Obsgrid was used to create the initial conditions for Exp. ObIC. Exp. ObIC+ also included observations in the initial conditions, but did so using the modification to the Cressman scheme for moisture described in Section 4.4. All experiments not described in this paragraph also used this modification.

Data assimilation was applied via observation nudging for some experiments, but with two variations among these experiments. The standard technique was used for Exp. ObIC+Nud4 and ObIC+Nud8, while the modification to water vapor mixing ratio assimilation described in Section 4.3 was used for Exp. ObIC+Nud4+ and ObIC+Nud8+. The nudging weight (G), was set to 4×10^{-4} s^{-1} for Exp. ObIC+Nud4 and ObIC+Nud4+, but to 8×10^{-4} s^{-1} for Exp. ObIC+Nud8 and ObIC+Nud8+.

Table 1. Experimental Design. The table indicates the source of initial conditions is GFS and whether observations are incorporated via objective analysis (Y, N) and whether modifications are made to the Cressman method for moisture (M). The table also indicates whether nudging is applied (Y, N), whether the nudging method was modified for moisture (M), and the nudging weight.

Experiment Name	Initial Conditions		Nudging	
	GFS	Obs	Applied	Weight (G; s^{-1})
Control	X	N	N	
ObIC	X	Y	N	
ObIC+	X	M	N	
ObIC+Nud4	X	M	Y	4×10^{-4}
ObIC+Nud4+	X	M	M	4×10^{-4}
ObIC+Nud8	X	M	Y	8×10^{-4}
ObIC+Nud8+	X	M	M	8×10^{-4}

6. RESULTS

The introduction of very dry conditions through the incorporation of observations into the initial conditions is discussed in 6.1. Unusual dryness introduced through the observation nudging is discussed in 6.2.

6.1 Initial Conditions

Unusually dry conditions can be introduced into WRF through the initial conditions. For example, Figure 1 shows the dewpoint at model level 15 at the initial time (12 UTC) on 16 February 2012. Using the GFS data alone for initial conditions (Exp. Control; Figure 1a) yields one area with very dry conditions over the Pacific Ocean (at approximately 29N 122W); the minimum dewpoint in this area is approximately -78C. This is well below the climatological 0.1 percentile value of -47C for this level (approximately 850 hPa) derived as described in section 4.1.

The inclusion of observations in the initial condition analysis via Obsgrid (Exp. ObIC; Figure 1b) results in more extensive dry regions for this example. A much larger area of relatively low dewpoints are now found along the western edge of the domain. Also, now there are two additional areas at this time and model level with low dewpoints: 1) over the Pacific Ocean at about 33N 122W where the minimum dewpoint is approximately -78C at approximately 850 hPa, and 2) along the Arizona-Mexico border around 111W where the minimum dewpoint is approximately -80C at approximately 700 hPa. For this model level at this time the percentage of grid cells whose dewpoint falls below the climatological 0.1-percentile value increases with the inclusion of observations in the initial conditions (i.e., Exp. Control to Exp. ObIC) from 1.13 to 8.50% (not shown).

The overall scope of the problem can be examined by looking at the percentage of model grid points below the 350 hPa level that have a dewpoint less than the 0.1 percentile value in Figure 2. For Exp. Control (Figure 2a), the time series of this quantity indicates that most of the cases stay below 0.2%, but that 16 February starts out around 0.5% and then falls. Incorporating observations into the initial conditions via Obsgrid (Figure 2b; Exp. ObIC) notably increases the percentage of very dry model grid points; all experiments start out at or above about 0.5%, but 16 February starts out above 1.5%. Note that for all experiments the prevalence of dry model grid points decreases with time.

Incorporating the altered analysis scheme for the relative humidity field described in Section 4.4 allows one to gain the benefits of incorporating observations in the initial conditions while not introducing the very dry spots found with the standard analysis technique. First, consider the example from the 16 February case where including observations into the initial conditions resulted in notable drying on model level 15 and the formation of two additional very dry spots (Figure 1b vs. Figure 1a). The altered analysis scheme (Exp. ObIC+) results in the removal of all very dry spots at this time and model level (Figure 1c) for this case; the domain minimum dewpoint is now approximately -48 C instead of the -80 C minimum in Exp. ObIC. Note that the structure of the dewpoint field at this level in Exp. ObIC+ matches the structure of Exp. ObIC better than it matches Exp. Control, with the major difference being the lack of very dry conditions in Exp. ObIC+.

Examining the domain mean time series of grid points below the 350 hPa level for Exp. ObIC+ (Figure 2c) shows that very few of the model grid points are less than the 0.1-percentile value (less than 0.1%). Comparing this to the standard analysis method (Exp. ObIC; Figure 2b) demonstrates the ability of the altered

analysis scheme to greatly minimize very dry conditions in the initial conditions.

Comparison of these experiments to observations (not shown) indicates that modifying the moisture analysis technique to avoid overdrying does not adversely affect the model forecast. Although the fit of the initial condition analysis to the observations is degraded above 1000 m AGL, during the forecast the model performs at least as well (or slightly better) than when using the original method.

6.2 Data Assimilation

Observation nudging can introduce unrealistically dry areas in WRF, even when the initial conditions are created by the altered analysis methodology from 6.1. An example of this is Figure 3d, which shows the dewpoint from Exp. ObIC+Nud8 on 1 March at 13 UTC at model level 16. There is an area with very low dewpoints just offshore of southern California (at this location model level 16 is approximately 825 hPa, 1600 m MSL). In the middle of this area model water vapor mixing ratios drop to 0. The absence of the dry spot from the analogous experiment without data assimilation (Exp. ObIC+; Figure 3a) indicates that the observation nudging is contributing to this dry spot.

Further investigation reveals that the 12 UTC San Diego rawinsonde is the specific observation that leads to the dry spot. Around 825 hPa this rawinsonde results in nudging towards dryer conditions. The appearance of cloud water by 13 UTC in the non-nudging experiment in the vicinity of San Diego indicates that the physical tendency terms are working to increase the moisture at this point. Therefore, compared to a case where the physical tendency terms are zero, the data assimilation is less effective in decreasing the error, and thus the innovation and the nudging tendency term will not decrease as rapidly with time. Just to the west of San Diego, the model does not form clouds by 13 UTC, suggesting that a smaller time-integrated correction would be effective in introducing drying here than is needed at San Diego. Because the innovation is calculated at San Diego, where the physical tendency terms work to counteract the drying from nudging during this period, and then the innovation is applied to an area that includes the area west of San Diego where the physical tendency terms do not appear to as effective in counteracting drying during this period, the data assimilation removes all moisture in a limited area west of San Diego at this model level by 13 UTC.

Because observation nudging is causing the bulk of the remaining excessively dry areas in the WRF experiments, the first potential solution we explore is decreasing the influence of observation nudging on the solution by decreasing the strength of the observation nudging. When the nudging weight is decreased by half to 4×10^{-4} s^{-1}, the very dry area just west of San Diego is no longer present at 13 UTC on model level 16 (Exp. ObIC+Nud4; Figure 3b). Compared to the experiment without any nudging (Exp. ObIC+; Figure 3a) the model is drier just west of San Diego, but the extreme dryness predicted with the stronger nudging weight is absent. The overall distribution of sub-0.1 percentile dewpoints below 350 hPa for the five case days (Figure 4) indicates that the weaker nudging strength is not sufficient to completely resolve the excessive dryness introduced by observation nudging. Observation nudging assumes that the tendency term introduced via nudging is smaller in magnitude than the physical tendency terms; this allows the model to maintain physically consistent conditions. However, compared to other variables, moisture may be more easily nudged to a physically unrealistic value given the large spatial variability in water vapor mixing ratio as compared to its absolute magnitude in combination with the fact that zero or near-zero water vapor mixing ratios in the lower atmosphere are physically unrealistic.

To address this issue, the modification to observation nudging described in Section 4.3 is applied to both the experiment with the weaker nudging (Exp. ObIC+Nud4) and with the stronger nudging (Exp. ObIC+Nud8). In the area west of San Diego that was very dry at 13 UTC in Exp. ObIC+Nud8 (Figure 3d), the observation nudging modification (Exp. ObIC+Nud8+; Figure 3e) results in much moister conditions, while allowing the overall dewpoint field to remain very similar to Exp. ObIC+Nud8. For the weaker nudging, even with the standard technique (Exp. ObIC+Nud4; Figure 3b) there was not an excessively dry area west of San Diego at 13 UTC on model level 16, but the new technique (Exp. ObIC+Nud4+; Figure 3c) decreases the drying that did occur in that location, while keeping the overall dewpoint field very similar. Examining the statistics for all model grid points below the 350 hPa level, the new technique reduces the percentage of points with dewpoint below the 0.1 percentile to below 0.2% for all experiments (Figure 4).

Verification of model dewpoint against observations (not shown) indicates that observation nudging improves the model results, while the modification to the observation nudging technique for moisture has limited effect on overall dewpoint MAE. Therefore, the modification effectively mitigates the introduction of very dry conditions via nudging without degrading the overall model forecast.

7. SUMMARY AND CONCLUSIONS

Both using the objective analysis in Obsgrid to incorporate observations in the initial conditions and using observation nudging can introduce areas with very dry conditions into WRF-ARW simulations. The large spatial variability in water vapor mixing ratio compared to its magnitude and the fact that there is always some moisture in the lower atmosphere (i.e., a water vapor mixing ratio of zero is unrealistic) may make it easier for nudging to cause unrealistic values in moisture than in other variables. Applying both a modification to the

relative humidity analysis methodology in Obsgrid and a modification to the water vapor mixing ratio observation nudging largely eliminates excessively dry conditions from the WRF solution. These modifications do not degrade the overall model dewpoint forecast. In addition to the modifications, applying the observation nudging more weakly (4×10^{-4} s^{-1} rather than 8×10^{-4} s^{-1}) also mitigates the formation of very dry areas. Quality control of moisture observations is also important for ensuring that observations do not cause excessively dry model conditions.

8. ACKNOWLEDGEMENTS

AirDat LLC provided TAMDAR observational data that expanded the above-surface data available for data assimilation and verification. This study was made possible in part due to the data made available to the National Oceanic and Atmospheric Administration by various providers for inclusion in MADIS. The RTMA use and reject lists were provided by Steve Levine at NCEP-EMC and greatly facilitated making full use of the MADIS observational dataset. The madis2littler tool was provided by Ruifang Li at NCAR. The first author was supported by a National Research Council postdoctoral associateship at the Army Research Laboratory for part of this research.

9. REFERENCES

Ardao-Berdejo J., and D. R. Stauffer, 1996: On the relative contribution of the Newtonian relaxation term in a nonhydrostatic mesoscale model used for dynamic analysis. In: 11th AMS conference on numerical weather prediction, Norfolk, Virginia, USA, pp 200–202.

Dee, D. P., and A. M. da Silva, 2003: The Choice of variable for atmospheric moisture analysis. *Mon. Wea. Rev.*, **131**, 155–171.

Deng, A., D. Stauffer, B. Gaudet, J. Dudhia, C. Bruyere, W. Wu, F. Vandenberghe, Y. Liu, and A. Bourgeois, 2009: Update on WRF-ARW end-to-end multi-scale FDDA system. 10th WRF Users' Workshop, NCAR, 23-26 June, Boulder, CO. 1.9. 14 pp.

De Pondeca, M. S. F. V., and Coauthors, 2011: The Real-Time Mesoscale Analysis at NOAA's National Centers for Environmental Prediction: Current Status and Development. *Wea. Forecasting*, **26**, 593–612.

Gao, Feng, Xiaoyan Zhang, Neil A. Jacobs, Xiang-Yu Huang, Xin Zhang, Peter P. Childs, 2012: Estimation of TAMDAR Observational Error and Assimilation Experiments. *Wea. Forecasting*, **27**, 856–877.

Gemmill, W., B. Katz, and X. Li, 2007: Daily real-time, global sea surface temperature—High-resolution analysis: RTG_SST_HR. NOAA/NWS/NCEP/MMAB Office Note 260, 39 pp. [Available online at http://polar.ncep.noaa.gov/mmab/papers/on260/sst_office_note.pdf].

Janjić, Z. I., 2002: Nonsingular Implementation of the Mellor–Yamada Level 2.5 Scheme in the NCEP Meso model, *NCEP Office Note*, No. 437, 61 pp.

Lee, Jared A., Walter C. Kolczynski, Tyler C. McCandless, Sue Ellen Haupt, 2012: An Objective Methodology for Configuring and Down-Selecting an NWP Ensemble for Low-Level Wind Prediction. *Mon. Wea. Rev.*, **140**, 2270–2286.

National Operational Hydrologic Remote Sensing Center, 2004. *Snow Data Assimilation System (SNODAS) Data Products at NSIDC*. Boulder, Colorado USA: National Snow and Ice Data Center. http://dx.doi.org/10.7265/N5TB14TC

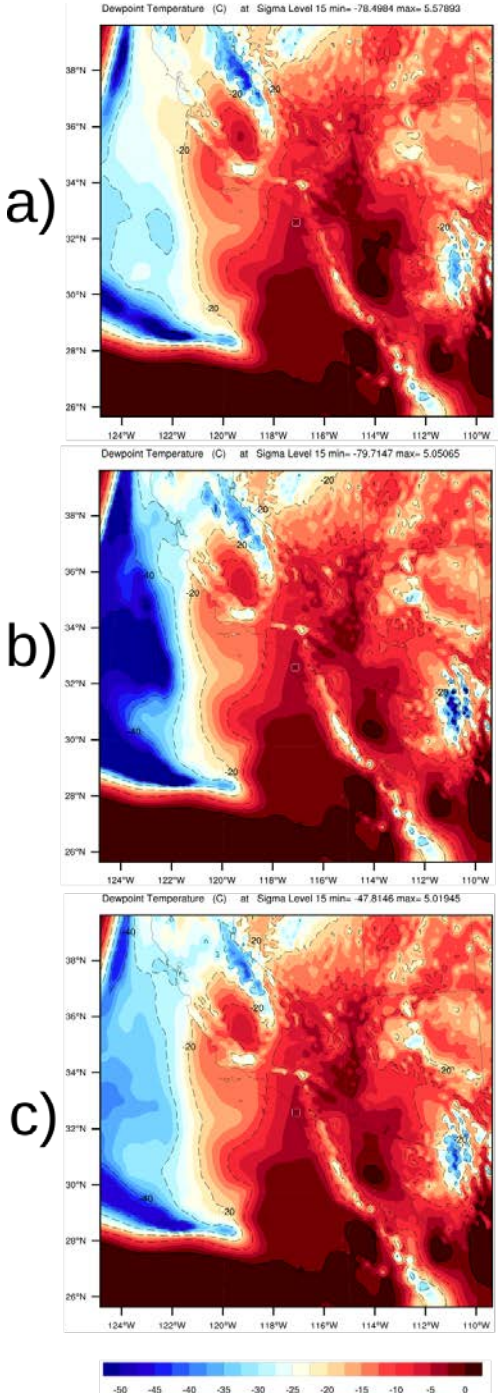

Figure 1. Dewpoint (C) for Exps. a) Control, b) ObIC, and c) ObIC+ on 16 February at 12 UTC at WRF-ARW model level 15. Note that all values less than -50 C are shaded in the same dark blue. The plotting routine treats all dewpoints less than ~-80 C as -80 C which prevents "singularities" where the water vapor mixing ratio goes to or approaches zero. Black contour lines are plotted every 10 C; these lines are dashed for negative values.

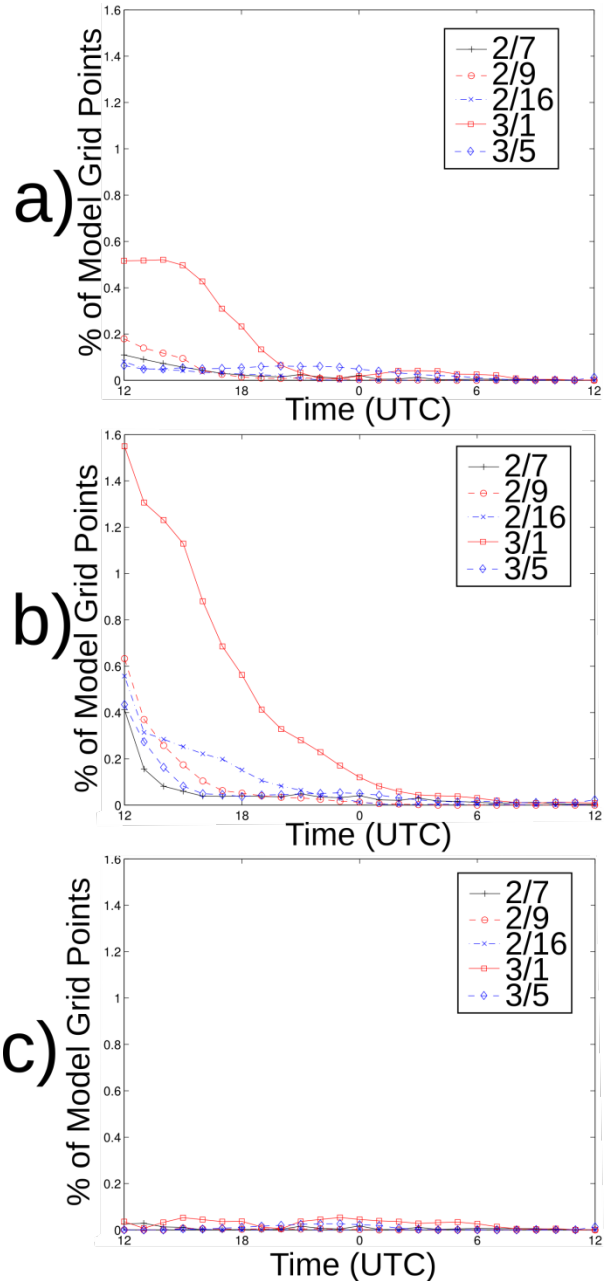

Figure 2. Time series of the percentage of WRF grid points below 350 hPa that fall below the 0.1 percentile climatological value for that pressure bin for Exps. a) Control, b) ObIC, and c) ObIC+.

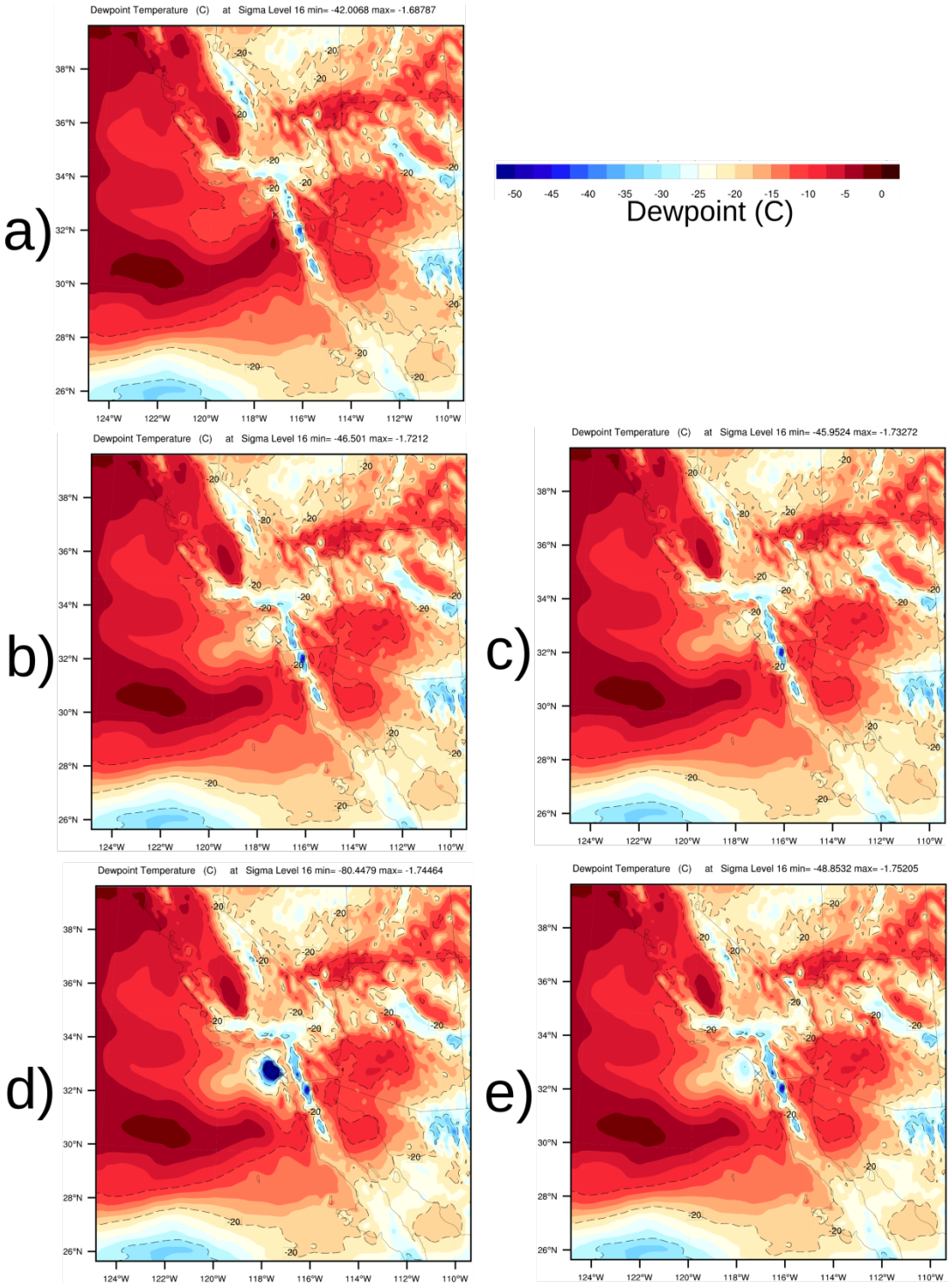

Figure 3. Dewpoint (C) for Exps. a) ObIC+, b) ObIC+Nud4, c) ObIC+Nud4+, d) ObIC+Nud8 and e) ObIC+Nud8+ on 1 March at 13 UTC at model level 16. Note that all values less than -50 C are shaded in the same dark blue. The plotting routine treats all dewpoints less than ~-80 C as -80 C which prevents “singularities” where the water vapor mixing ratio goes to or approaches zero. Black contour lines are plotted every 10 C; these lines are dashed for negative values. The black “X” on the eastern edge of the dry spot marks the location of the San Diego, CA, rawinsonde location.

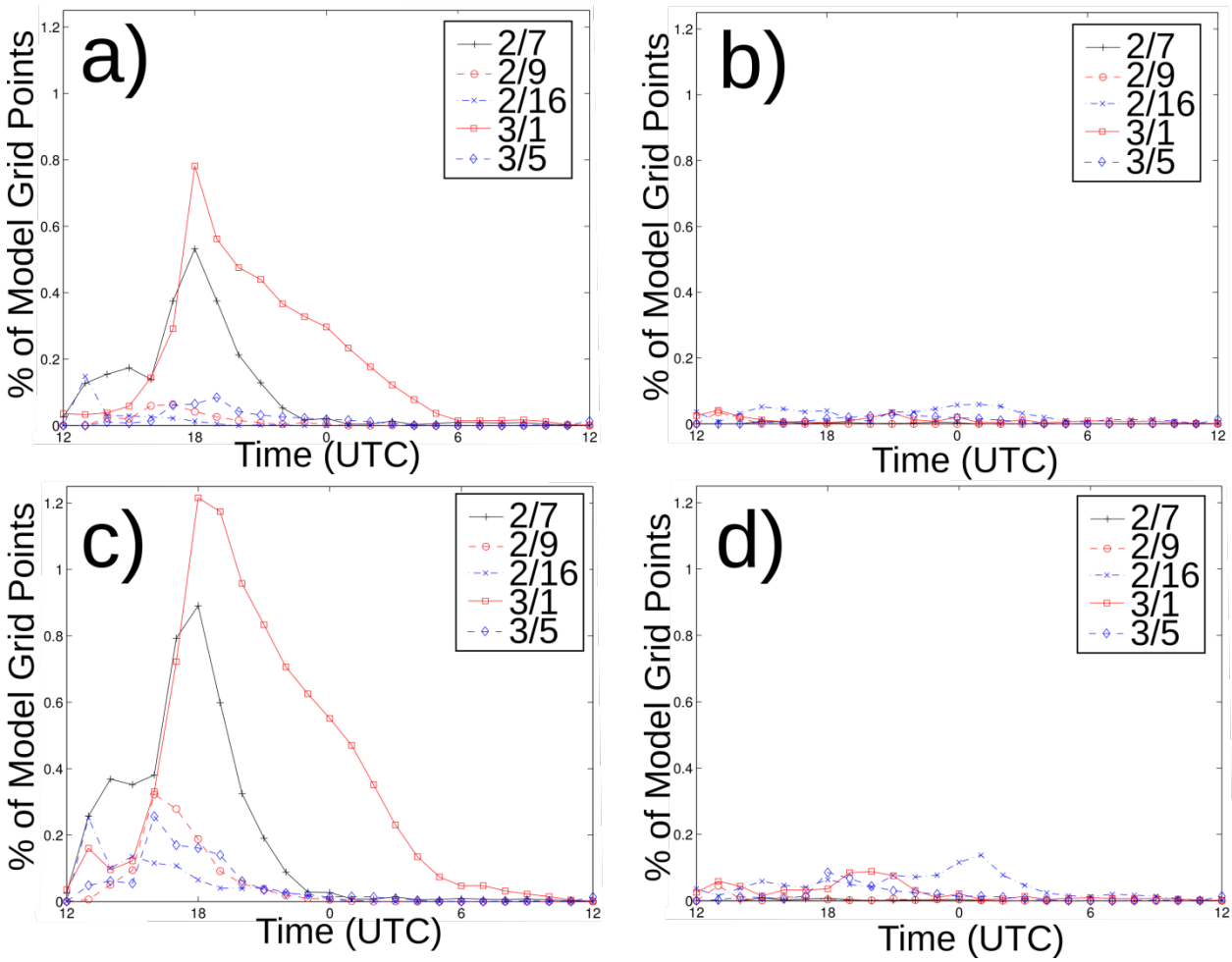

Figure 4. Time series of the percentage of WRF grid points below 350 hPa that fall below the 0.1 percentile climatological value for that pressure bin for Exps. a) ObIC+Nud4, b) ObIC+Nud4+, c) ObIC+Nud8, and d) ObIC+Nud8+.